Marco, M.; Belda, R.; Miguélez, MH.; Giner Maravilla, E. (2018). A heterogeneous orientation criterion for crack modelling in cortical bone using a phantom-node approach. Finite Elements in Analysis and Design. 146:107-117. https://doi.org/10.1016/j.finel.2018.04.009

A heterogeneous orientation criterion for crack modelling in cortical bone using a phantom-node approach

Miguel Marco[1], Ricardo Belda[2], María Henar Miguélez[1], Eugenio Giner[2*]

[(1)] Department of Mechanical Engineering. Universidad Carlos III de Madrid. Avda. de la Universidad 30, 28911 Leganés, Madrid, Spain

[(2)] Centre of Research in Mechanical Engineering – CIIM, Department of Mechanical and Materials Engineering, Universitat Politècnica de València Camino de Vera, 46022 Valencia, Spain

** eginerm@mcm.upv.es corresponding author*

Abstract

Cortical bone can be considered as a heterogeneous composite at microscopic scale, composed of osteons that act as reinforcement fibres embedded in interstitial matrix. Cement lines constitute the interface between osteons and matrix, and they often behave as the weakest links along which microcracks tend to propagate. However, current simulations of crack growth using XFEM combined with usual orientation criteria as implemented in commercial codes do not capture this behaviour: they predict crack paths that do not follow the cement lines surrounding osteons. The reason is that the orientation criterion used in the implementation of XFEM does not take into account the heterogeneity of the material, leading to simulations that differ from experimental results. In this work, a crack orientation criterion for heterogeneous materials based on interface damage prediction in composites is proposed and a phantom node approach has been implemented to model crack propagation. The method has been validated by means of linear elastic fracture mechanics (LEFM) problems obtaining accurate results. The procedure is applied to different problems including several osteons with simplified

geometry and an experimental test reported in the literature leading to satisfactory predictions of crack paths.

Keywords

Crack path; heterogeneous media; orientation criterion; phantom node method; bone fracture.

1. Introduction

The study of the mechanical response of bone is an active field of research for both biologists and engineers [1]. Bone fracture, principally caused by accidents, is a common trauma affecting young and elderly people. In an increasingly aging society, bone fracture (usually hip fracture) has a great social importance involving enormous costs [2, 3]. The understanding of bone fracture at different length scales is still a challenge and its modelling may reveal insight into the fracture behaviour of bone at microscale. In this field, finite element modelling can help to predict and analyse the crack path under different conditions. Finite element simulations are also used in other biomechanical areas, such as bone remodelling [4, 5].

Two main tissues can be distinguished within bone structure: the outer regions, composed of cortical bone and the inner regions composed of trabecular bone. The highly hierarchical structure of bone [6, 7] makes it necessary to develop multiscale models where the different scales must be properly modelled [8, 9]. On the one hand, cortical bone is a hard, dense and highly mineralised tissue, bearing the main compressive and bending loads. On the other hand, trabecular bone is made of a reticular, rod and plate-like structure tissue, that permit a global bone mass reduction and leads a high surface area suitable for metabolic reactions [10-13].

The role of cortical bone is crucial in the global fracture behaviour of bone. Its analysis at the microscale helps to the understanding of the macro fracture of long bones. At the microscale (50–500 μm), cortical bone is a heterogeneous material with non-isotropic properties that can be considered as a biological composite, composed of fibres with high stiffness (in terms of Young's modulus) embedded in a matrix [14]. The different constituents of cortical bone have dissimilar mechanical properties and this has a strong influence on the crack path at this scale. The basic structural unit of compact bone at the micro level is the osteon (also known as Haversian system) that has a complicated hierarchical morphology at a lower scale [6,11]. In this work, only the Haversian canal and the cement line will be considered. We distinguish three relevant constituents (shown in Fig. 1 at different scales):

- Secondary osteons: recent osteons formed in the continuous process of bone remodelling. Their diameter ranges between 50–200 μm and length in the range 3–5 mm [11, 15].
- Interstitial matrix: it is mainly composed of old osteons with high mineral content and about 10-15% higher stiffness than secondary osteons [16, 17].
- Cement line: a weak thin layer (about 1–5 μm thick [18]) surrounding the secondary osteons. The cement line constitutes the interface between secondary osteons and the interstitial matrix. This is a less mineralized zone which exhibits low toughness and stiffness properties, leading to propagation of cracks around secondary osteons [17-21].

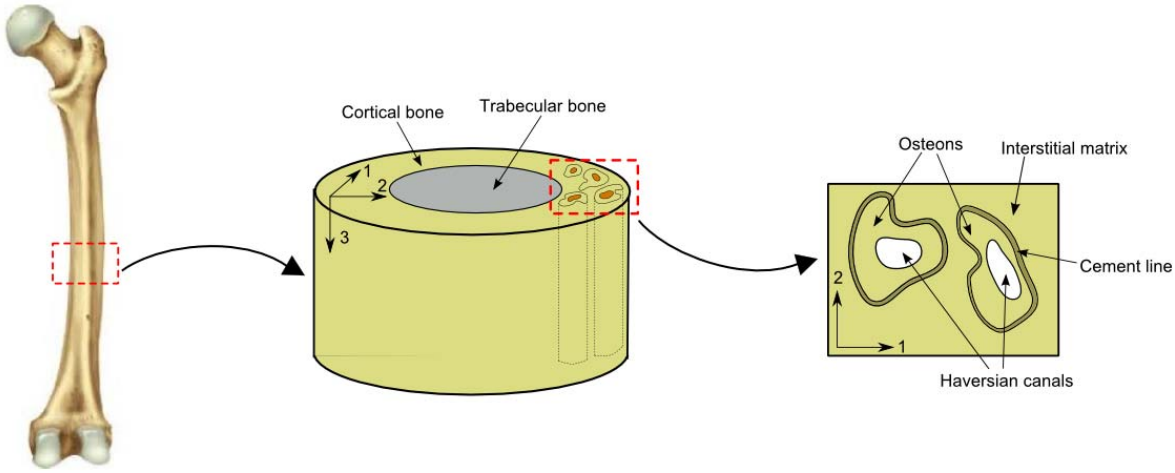

Figure 1. Scheme of the cortical bone structure from macroscopic to microscopic scale.

The cement line has been analysed in the literature for being the constituent at the microscale that shows the highest risk of failure in cortical bone tissue (see for instance [20-25]). Fig. 2 shows an example of the crack propagation path following cement lines, reported in [24]. This interface between osteons and the interstitial matrix is often origin of cracks and its most probable propagation path [7, 24, 26, 27], as it is a less mineralized tissue [20]. Some authors suggest that collagen fibres do not cross cement lines and thus it represents the weakest interface within the cortical bone tissue [22, 23]. This approach is consistent with the phenomenon observed experimentally by which microcracks tend to follow the cement lines rather than crossing osteons [28]. Similarly, Nobakhti *et al*. [18] analyzed the behaviour of cement lines in cortical bone tissue and claim that strain increases at these interfaces.

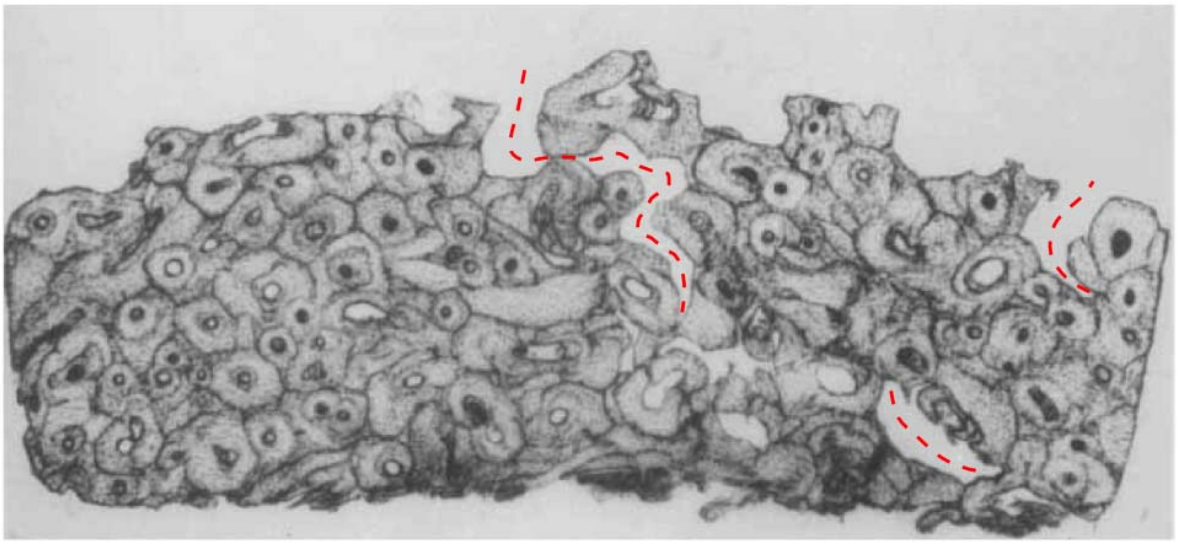

Figure 2. Crack propagation path following the weakened interfacial zone (cement line). The crack does not cross the cement line. The main cracks are marked in red colour dashed lines. Reprinted from [24] with permission of John Wiley and Sons.

Despite the interest of experimental studies, the simulation of bone fracture is still a challenge both at macroscopic and microscopic scale. Modelling crack propagation in cortical bone requires the implementation of techniques able to account for the heterogeneous nature of bone, and there is a lack of an appropriate criterion to predict fracture paths in this type of heterogeneous materials, as discussed in this section.

Budyn *et al*. [29] analysed the crack propagation in osteons using the extended finite element method (XFEM). They predefined initial cracks into osteons and studied the subsequent propagation based on the maximum tangential stress (MTS) criterion, which is commonly used for homogeneous materials. The predicted crack path is straight and orthogonal to the prescribed displacement, without detecting the presence of heterogeneities such as the cement lines. The predicted path that crosses osteons is probably due to the propagation criterion used, which is not suitable for heterogeneous materials. Similar fracture paths were obtained in [30] accounting also for the effect of age in the porosity of the bone. Analogous results have been obtained by other authors

[31-33], without obtaining a realistic path. The above references applied fracture criteria initially conceived for homogeneous material. Also, XFEM combined with the MTS criterion is used in recent works [34], leading to non-realistic fracture paths, where the crack path is not affected by the presence of the cement line.

Guo *et al*. [35], applied principles of LEFM to study the dependence of fracture process on the material properties using a simplified model composed of an osteon and the interstitial matrix. Their results claim that low-stiffness osteons (newly formed) may toughen cortical bone tissue as microcracks tend to propagate towards them, limiting its growth [35].

Some authors have developed cohesive zone models to simulate material interface behaviour at different length scales in bone [9,36-39]. For example, Lin *et al*. [36] recently defined a cohesive zone model to define the mechanical behaviour at the nanoscale of the extrafibrillar matrix in bone, the interfacial interactions in a simplified hexagonal-based model under compression loading [36]. On the other hand, Cox and Yang [39] formulated a cohesive fracture model and applied it to human femoral cortical bone data. They studied the viability of assuming LEFM in cortical bone fracture, claiming that it only can be assumed when crack is longer than a certain length scale.

Different multiscale approaches can be found that take into account the heterogenous microstructure [9,40-42]. Ural and Mischinski [9] developed a multiscale approach of bone fracture investigating the influence of bone microstructure properties on macroscale fracture. They used a computational fracture mechanics approach based on cohesive finite element modelling. At microscale, Ural *et al*. evaluated two different models: 2D finite element models created from human cortical bone microscopy images to determine the influence of cement line properties on the crack propagation path and finite element models of 3D compact tension test specimens with idealized geometry. The macroscale

simulations evaluated the fracture load of an idealized radius bone, incorporating the fracture toughness and critical strength values estimated at the microscale [9]. Vernerey and Kabiri [40,41] proposed an adaptive multiscale formulation to model fracture in heterogeneous media, providing both a concurrent microscopic and macroscopic description adaptively as fracture proceeds. Their approach consists in defining coarse finite elements in the macroscopic domain, while refining the mesh in high strained areas, coupling the embedded representative volume elements (RVE) with the rest of the domain. In [41] they use an XFEM modelling of crack propagation. Souza and Allen [42] highlighted the importance of defining the crack initiation and proposed a two-way coupled multiscale approach, where cohesive zones were modelled using an XFEM description.

Li *et al*. [43] performed an experimental study and numerical simulations of fracture processes to characterize fracture toughness in bovine femoral cortical bone tissue, focusing on spatial variability and anisotropy of its resistance to fracture. The experimental data was obtained using single-edge-notch-bending specimens of cortical bone tested in a three-point bending setup, while the numerical approach was developed using the XFEM method.

To the authors' knowledge, none of these works addresses the need of a criterion for heterogeneous microstructure to predict the proper angle of propagation to simulate fracture paths in cortical bone.

This paper focuses on the modelling of fracture propagation at the microscale taking into account its heterogeneous microstructure. In this work, the proposed criterion for crack propagation within a heterogeneous microstructure has been applied in combination with the Phantom Node Method (PNM). The Phantom Node approach has been implemented in the commercial FE code Abaqus by means of user's subroutines. For the

sake of simplicity, the PNM has been chosen instead of the standard XFEM because it is easier to implement in a commercial code (no degree-of-freedom enrichment is needed).

In this work, the simulation of simple cases corresponding to LEFM problems has allowed the validation of the implementation and assessment of its accuracy. Then, this procedure is employed to simulate crack propagation in cortical bone, with simplified and realistic bone microstructure morphologies, showing good correlation between experiments and numerical predictions.

The PNM was proposed by Hansbo and Hansbo [44]. In PNM, the crack is treated explicitly and crack opening and shearing are calculated based on displacements of both original and phantom nodes overlaid to some of the original nodes [44,45]. Similar to XFEM formulation, in PNM an element can be intersected by a crack, so fracture does not need to follow element sides. Moreover, as proved by Song [46], PNM is equivalent to standard XFEM which is based on the framework of partition of unity method. To date, this method has been applied to different LEFM problems, and also in composite materials such as FRP composites [45,47], but not in cortical bone at microscopic scale.

This work is organized as follows. After this introduction, the main features of the PNM implementation in a commercial code are explained and then, a validation of the implementation through LEFM problems is carried out. Then, the crack orientation criterion for heterogeneous materials is proposed. Using this criterion, different problems with idealized and realistic cortical bone geometry are simulated using the PNM, and compared to experimental results of the simulations carried out by other authors who used other methods. The conclusions of the work are presented in the last section.

2. Phantom Node Method (PNM) and validation

2.1. Phantom Node Method (PNM)

The PNM treats discontinuities explicitly, similar to XFEM, with only straight internal crack segments under consideration. A difference with XFEM is that PNM is not based on the enrichment of the FE model with additional degrees of freedom [48]. Considering the advantages of this feature of the PNM from the implementation viewpoint, we chose this approach over standard XFEM for the sake of simplicity. One disadvantage is that the crack tip enrichment cannot be included and that the crack must necessarily end at an element side. Often, this disadvantage is not critical because typically the mesh is sufficiently refined.

When a crack intersects an element, this element is duplicated. Then, the nodal connectivity of the two elements is modified, linking the elements to each side of the crack, respectively (see Fig. 3). The nodes that belong to the new elements but are not connected to the previous mesh are called *phantom nodes*. This allows the displacement discontinuity needed to reproduce the crack presence.

The new elements are subdivided into subdomains in order to carry out the numerical integration, which is performed at one side of the crack line only for each of these elements, being the crack one of the subdomain boundaries. Hence, the integrated subdomains match the previous domain of the problem. A quadrilateral element is either subdivided into two quadrilateral subdomains when the element is intersected through opposite faces or subdivided into triangular subdomains when contiguous faces are intersected. This subdomain division was used and explained by Möes *et al.* in [48].

The elements intersected by the crack are also named mathematical elements (MEs), which are only active in the region corresponding to the subdomain they represent [45].

A scheme of several elements intersected by a crack and PNM topology is shown in Fig. 3.

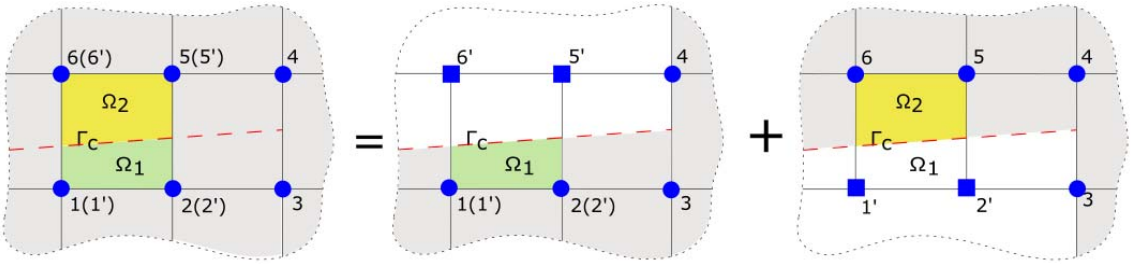

Figure 3. Scheme of a crack modelled by means of Phantom Nodes. Elements intersected by the crack are duplicated and divided into two subdomains (Ω_1 and Ω_2). In this figure real nodes are represented as circular markers and Phantom Nodes are represented as square markers. Connectivity between crack tip nodes 3 and 4 is kept active.

Thus, PNM is based on the topology modification of the elements intersected by a crack. This way, the new elements are connected to each of the sides of the crack line, respectively, allowing for the crack discontinuity. Only connectivity between crack tip nodes is kept active (nodes 3 and 4 in Fig. 3). The nodes of the crack tip element are only partially duplicated (nodes 2 and 5 are duplicated but 3 and 4 are not). Therefore, the crack tip will always be on the element side that connects the two nodes that are not duplicated.

The implementation of the PNM is carried out through a user element (UEL) subroutine in the FE commercial code Abaqus/Standard. Subroutine inputs are: intersection points between elements and crack face, intersection type (opposite or contiguous faces) and distance from nodes to crack tip. With these parameters, our UEL subroutine is able to subdivide each intersected element into subdomains, integrating the active subdomains and assembling their contribution to the FE global stiffness matrix. The identification of the intersection type, points of intersection between crack and

element sides, element duplication and modifications in the topology are carried out through different Python scripts developed by the authors.

When crack propagation is considered, it is necessary to estimate the new angle orientation for each crack increment. This postprocessing task is done by means of the output files treatment through a co-simulation between Abaqus/Standard and Python scripting. In these analyses, each crack increment involves a new simulation of the problem.

2.2. PNM validation

Different analytical problems from LEFM have been solved to validate the PNM. First, a mode I problem is considered, where we simulate an infinite array of collinear cracks under tensile traction in an infinite domain. Secondly, the Westergaard's problem is considered as a mixed mode crack problem. The aim of these analyses is to study the capabilities of the method and its robustness with different element sizes, in terms of stress intensity factor (SIF). In these problems SIF is calculated through the *J*-integral (in pure mode I) or through the interaction integral (in plane mixed mode behaviour). A sketch of each validation problem is shown in Fig. 4, where the shaded area is the domain numerically modeled.

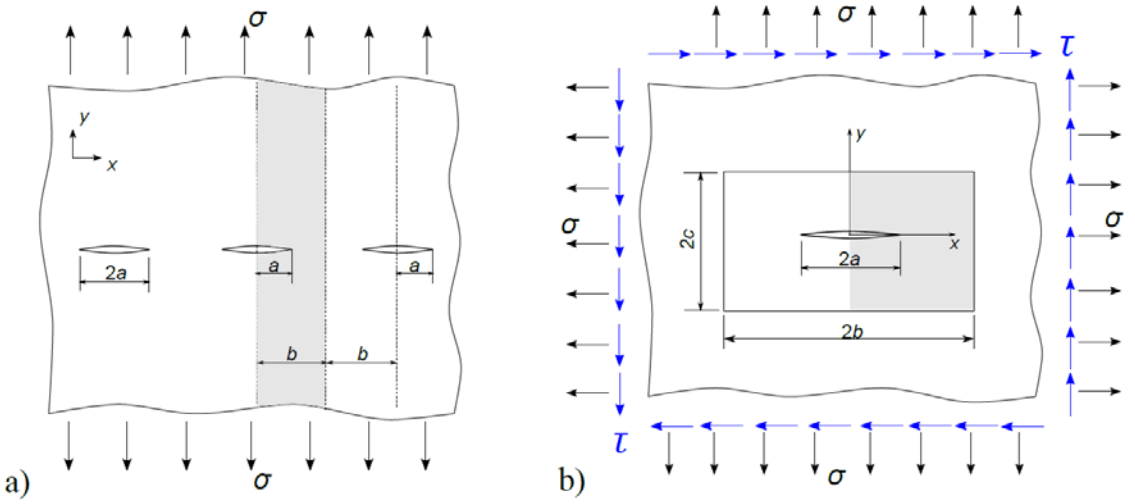

Figure 4. Sketches of the two problems used in the PNM validation: a) Infinite array of collinear cracks in tension. b) Westergaard's crack problem

2.2.1. Infinite array of collinear cracks in tension

This problem in pure mode I is used to obtain a first approximation regarding the dependence of the solution on the element size. Through Eq. 1 is possible to calculate the exact value of K_I in this problem [49]:

$$K_I = \sqrt{\frac{2b}{\pi a} tan\left(\frac{\pi a}{2b}\right)}\,\sigma\sqrt{\pi a} \tag{1}$$

where the different variables are shown in Fig. 4a. In this problem a=1 and b=2a. A sufficiently large domain is considered. The model dimensions are 12a in y-axis and 2a in x-axis. σ is taken as σ = 1/2 (units of pressure), in order to yield K_I = 1. The Young's modulus is E=10^7 (units of pressure) and the Poisson's ratio is v = 0.333. A plane stress hypothesis is assumed, using quadrilateral elements (coded CPS4 in Abaqus). Boundary conditions simulate the periodic symmetry of the problem, so the lateral nodes of the domain represented in Fig. 4a are constrained in the X-direction. Using these boundary conditions the domain of an infinite array of collinear cracks in tension is reproduced.

In this problem, four meshes are used, with element sizes equal to: $a/2$, $a/4$, $a/8$ and $a/16$. The different meshes and contour results in terms of σ_{yy} are shown in Fig. 5a.

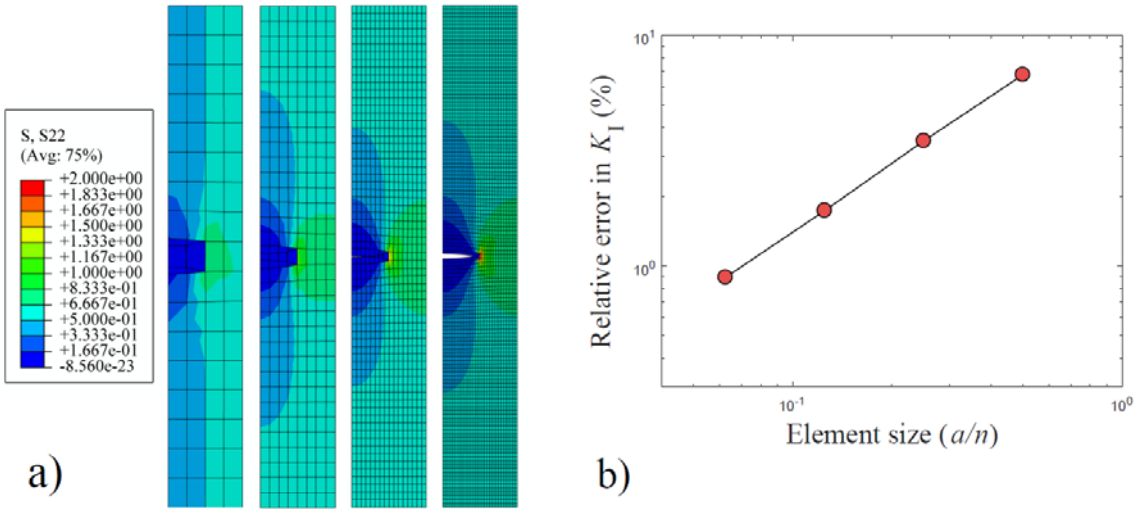

Figure 5. Infinite array of collinear cracks in tension. a) Different meshes. Plot of σ_{yy} stress field; b) Relative error in K_I depending on element size.

In Fig. 5a, the degree of refinement can be appreciated, showing that fine meshes are able to capture the fracture effects ahead the crack tip. The relative error obtained for K_I (in percentage) obtained with the PNM is plotted in Fig. 5b. Results provide a good approximation to the exact value of K_I for the problem of an infinite array of collinear cracks in tension problem when PNM is used. It can be seen that the relative error is about 1% when the smallest element size is used (element size=$a/16$). Results in this validation problem provide a good approximation to the exact value in mode I.

2.2.2. Westergaard's crack problem

A problem in mixed mode behaviour with an exact solution has also been solved for different element sizes in order to analyse the accuracy of the PNM. The problem analysed is an infinite plate with a crack of finite length, and it has been also used to

validate other approaches, such as XFEM [50]. The sketch of the problem is shown in Fig. 4b. Crack length is 2a, and the domain is biaxially loaded with remote uniform tractions for mode I and remote uniform shear for mode II (see Fig. 4b). Exact solutions for the SIFs of this problem are: $K_{\mathrm{I,ex}} = \sigma\sqrt{\pi a}$ and $K_{\mathrm{II,ex}} = \tau\sqrt{\pi a}$.

Using explicit expressions for the stress field in terms of spatial coordinates derived in [51], it is possible to compute equivalent nodal forces for a finite portion of the domain. These nodal forces are represented in Fig. 6a. For biaxial loading with remote uniform traction σ, the stress field at a point (x,y) associated with mode I loading is:

$$\sigma_{\mathrm{xx}}^{\mathrm{I}} = \frac{\sigma}{\sqrt{|t|}}\left[\left(x\cos\frac{\Phi}{2} - y\sin\frac{\Phi}{2}\right) + y\frac{a^2}{|t|^2}\left(m\sin\frac{\Phi}{2} - n\cos\frac{\Phi}{2}\right)\right] \tag{2a}$$

$$\sigma_{\mathrm{yy}}^{\mathrm{I}} = \frac{\sigma}{\sqrt{|t|}}\left[\left(x\cos\frac{\Phi}{2} - y\sin\frac{\Phi}{2}\right) - y\frac{a^2}{|t|^2}\left(m\sin\frac{\Phi}{2} - n\cos\frac{\Phi}{2}\right)\right] \tag{2b}$$

$$\sigma_{\mathrm{xy}}^{\mathrm{I}} = y\frac{a^2\sigma}{|t|^2\sqrt{|t|}}\left(m\cos\frac{\Phi}{2} + n\sin\frac{\Phi}{2}\right) \tag{2c}$$

And for loading with remote uniform shear traction τ (mode II) the stress field at points (x,y) belonging to the half plane $x\geq 0$ are given by:

$$\sigma_{\mathrm{xx}}^{\mathrm{II}} = \frac{\tau}{\sqrt{|t|}}\left[2\left(y\cos\frac{\Phi}{2} + x\sin\frac{\Phi}{2}\right) - y\frac{a^2}{|t|^2}\left(m\cos\frac{\Phi}{2} + n\sin\frac{\Phi}{2}\right)\right] \tag{3a}$$

$$\sigma_{\mathrm{yy}}^{\mathrm{II}} = y\frac{a^2\tau}{|t|^2\sqrt{|t|}}\left(m\cos\frac{\Phi}{2} + n\sin\frac{\Phi}{2}\right) \tag{3b}$$

$$\sigma_{\mathrm{xy}}^{\mathrm{II}} = \frac{\tau}{\sqrt{|t|}}\left[\left(x\cos\frac{\Phi}{2} - y\sin\frac{\Phi}{2}\right) + y\frac{a^2}{|t|^2}\left(m\sin\frac{\Phi}{2} - n\cos\frac{\Phi}{2}\right)\right] \tag{3c}$$

where m, n, $|t|$ and Φ are real-valued functions of x and y coordinates, defined as

$$m = \mathrm{Re}t = x^2 - y^2 - a^2 \tag{4}$$

$$n = \mathrm{Im}t = 2xy \tag{5}$$

$$|t| = |m + in| = \sqrt{m^2 + n^2} \tag{6}$$

$$\Phi = \arg\bar{t} = \arg(m - in) \qquad \text{with } \Phi \in [-\pi, \pi] \tag{7}$$

In this problem, crack length is a=1 and the finite domain dimensions are b=2a, c=a. Five uniform meshes have been used, with element sizes equal to: a/4, a/8, a/16, a/32 and a/49. Nodal equivalent forces (shown in Fig. 6a) are those that yield $K_{I,ex}$ = $K_{II,ex}$ = 1. As in the previous problem, the Young's modulus is E=10^7 (units of pressure), the Poisson's ratio is v=0.333 and plane stress conditions are assumed (element CPS4 in Abaqus).

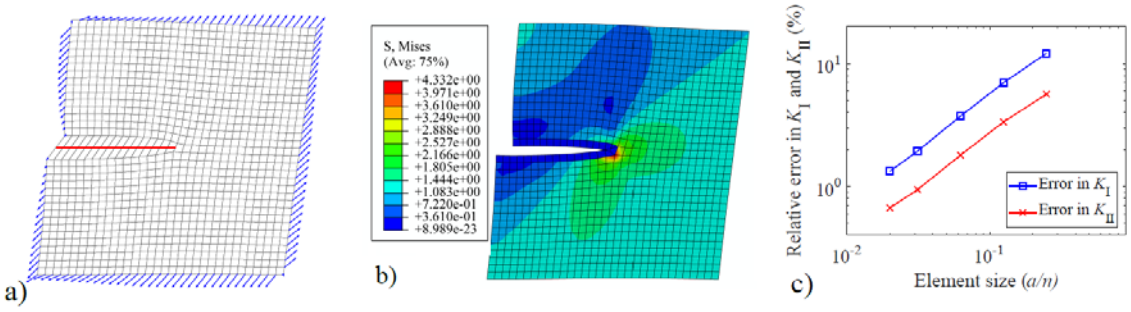

Figure 6. Westergaard's crack problem. a) Sketch of the problem with nodal forces for the third mesh of the sequence (element size equal to a/16). b) von Mises contour plot for the same mesh of the sequence. c) Relative error in K_I and K_{II} (in percentage).

The relative error in K_I and K_{II} estimation is plotted in Fig. 6c. Results show that the method is accurate enough in problems with mixed mode behaviour, reaching errors in SIFs of about 1%. These results validate the proposed method for 2D problems.

3. Modelling fracture in cortical bone

Once our implementation of the PNM has been validated, it will be applied to simulate problems of crack propagation. In this section, 2D fracture of cortical bone at the microscale is simulated for different morphologies of transversal sections.

3.1. Crack orientation criterion

Crack orientation criteria are necessary to predict the crack growth direction in simulations of crack propagation problems. Usually, for homogeneous materials and proportional loading conditions, the MTS criterion provides good results. Since cortical bone is a heterogeneous material that can be considered as a composite material with a reinforced microstructure [14], it is necessary to establish a proper crack orientation criterion that takes into account this heterogeneity. In this material, secondary osteons play the role of reinforcement fibres, embedded in the interstitial matrix, and cement lines act as the interface between fibres and matrix. In order to take into account the influence of the microscopic bone morphology, we have developed and applied a crack orientation criterion that considers the interface damage in structural composites (as proposed in [52]). According to [52], to predict the interface damage in a composite material, it is necessary to analyse the stresses ahead the crack tip, and to compare them with the critical stresses for each constituent of the composite.

The type of failure in the composite depends on the critical strengths of the materials and their relative values. Hull *et al*. [52] propose relationships between stresses near the crack tip and ultimate strength of the constituents that determine the failure either in the matrix, in the interface or in the fibre. In following discussion, subscripts 1 and 2 refer to the parallel and transverse direction respect to the fibres respectively, and S_1, S_2 and S_{12}, denote the ultimate strength limit in the corresponding direction (1, 2 or shear strength in the 1-2 plane). In these relationships, σ_1 is the actual stress in the fibres direction and σ_2

is the stress orthogonal to the fibres direction, both at the crack tip. S_1 is the uniaxial strength parallel to the fibres direction, S_2 is the uniaxial strength in the orthogonal direction and S_{12} is the intralaminar shear strength in the fibres plane.

When a brittle and sharp crack encounters a fibre, as shown in Fig. 7a, different fracture types can appear depending on the relative values of the constituent and interface strengths. In the crack tip region, different stresses exist (shown in Fig. 7b): σ_1 tends to cause fibre failure, σ_2 tends to cause interfacial fracture by tensile traction and τ tends to produce interfacial fracture by shear stress. Hull *et al*. propose different relationships between stresses in the vicinity of the crack tip and ultimate strengths of the composite to determine the type of fracture. They propose three situations about interface fracture (Fig. 7c):

- When $S_1/S_2 > \sigma_1/\sigma_2$ interface cracking due to tensile traction normal to the interface will appear prior to fibre failure.
- When $S_1/S_{12} > \sigma_1/\tau_{12}$ interface cracking due to shear stress will appear along the interface prior to fibre failure.
- When $S_{12}/S_2 > \tau_{12}/\sigma_2$, interface cracking will be more favourable due to transverse tensile traction than due to shear stress. Only if these relationships are not satisfied, crack will grow across the fibre.

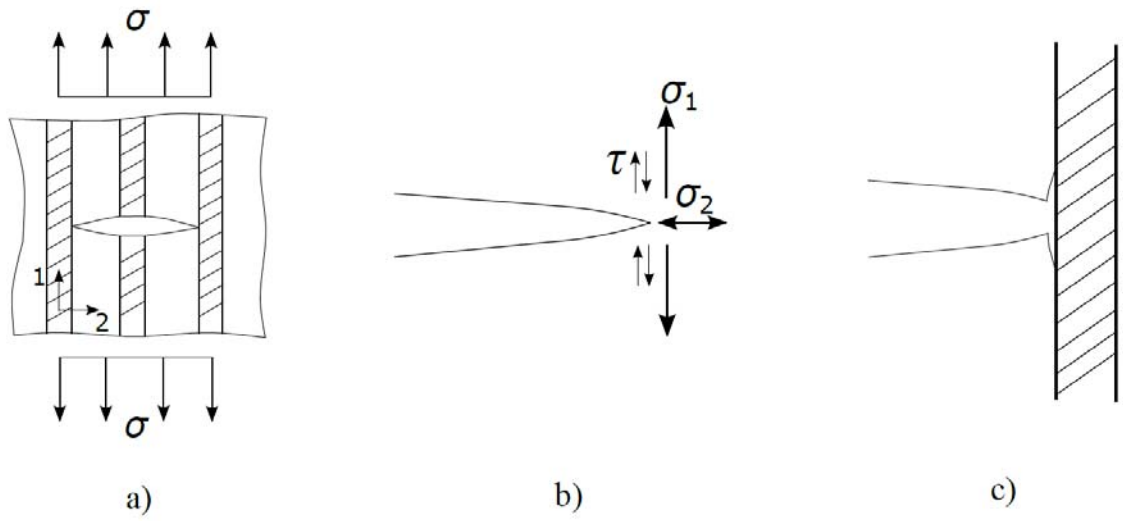

Figure 7. Brittle fracture close to fibres and stresses ahead the crack tip. a) Brittle fracture matrix close to the fibre. b) Stresses ahead the crack tip. c) Interface fracture.

Following this approach, the criterion proposed in this work consists in analysing the critical stresses ahead the crack tip as a function of the constituent and applying the MTS criterion methodology when the crack propagates within a single material. Therefore this criterion constitutes a simple method that can be applied to crack propagation problems in heterogeneous or composite materials.

In Fig. 8a we show a scheme of the proposed criterion. For the application of the orientation criterion, circumferential stresses divided by critical stress of the corresponding constituent are computed ahead the crack tip at integration points of each element in a region of interest surrounding the crack tip. Due to discretization errors, integration points in the element close to the crack tip are discarded for the stress computation. In this work, full integration of elements is used. This way, the number of integration points available is 4 per element for the quadrilateral elements used in this work. The angle of propagation at each crack growth step will be the one for which f reaches a maximum value.

Fig. 8b shows a step of the propagation in an osteon, in which the crack tip is at the cement line. The red line shows the crack faces in this simulation. In the postprocessing stage, the parameter *f* is computed in the area of interest highlighted in Fig. 8b) and the next angle of propagation is the one for which the parameter *f* is the greatest. In this particular example and taking into account the strength limits of the different constituents, the most probable propagation angle is the one that follows the cement line.

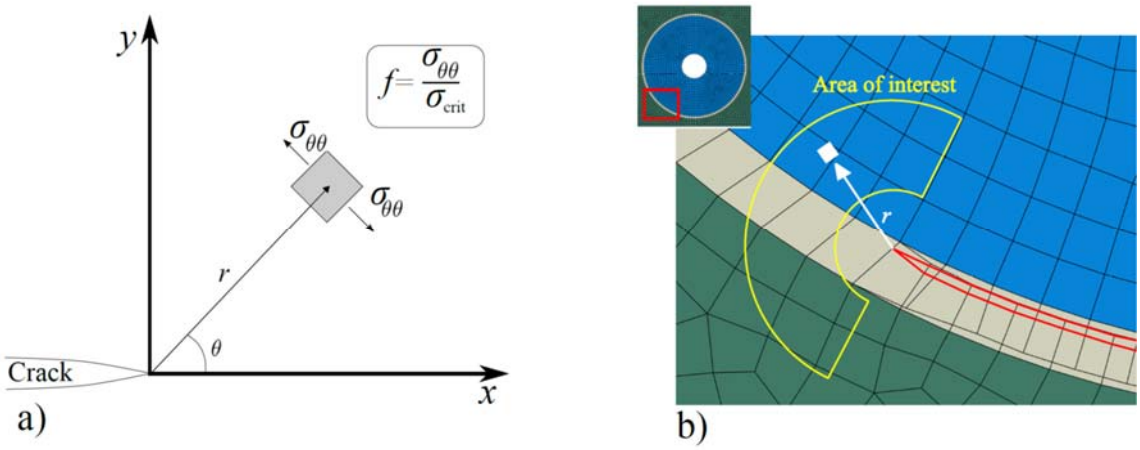

Figure 8. Crack orientation criterion developed in this work for fracture in cortical bone. Parameter *f* is calculated ahead the crack tip in a region of interest, and fracture is propagated in the direction where *f* reaches the maximum value. a) Scheme of the crack orientation criterion proposed in this work; b) Detail of the region of interest, showing a given step with the crack tip at the cement line as an example.

Through this criterion, not only the principle of the MTS criterion is considered, but also the ultimate mechanical properties of each constituent, which are necessary for the correct crack path prediction in heterogeneous materials.

3.2. Application to simplified geometries of cortical bone

One of the goals of this paper is to reproduce realistic fracture paths found in a transversal section of cortical bone considering its morphology at the microscale. First, osteon-like structures with simplified geometry are modelled in order to test the PNM and

the crack orientation criterion proposed. Finally, the method is applied to simulate crack propagation in realistic microstructural morphologies of cortical bone.

In what follows, we define the mechanical properties of the constituents under analysis. As explained in Section 1, we consider the following three main constituents: secondary osteons, interstitial matrix and cement lines. In the literature there is a wide dispersion regarding bone mechanical properties [21,25,53,54]. This scatter in the material properties can also affect to the numerical estimation of bone fracture load [55].

Given the problem conditions of our study, the mechanical properties of cortical bone components (cement line, interstitial matrix and secondary osteons) used in our numerical models are shown in Table 1. These values as well as their physical dimensions are inputs in the simplified and realistic numerical models shown in this section. Poisson's ratio has been assumed as ν=0.3 for each component, since it is usually close to this value in the literature [16,18,56-60]. Table 1 summarizes different mechanical properties available in literature.

Table 1. Summary of the mechanical properties and dimensions of constituents in cortical bone.

Component	***E* (MPa)**	**σ_{crit} (MPa)**	**G_c (N/m)**	**Dimensions (μm)**
Osteon	13290 [19]	100 [11]	860 [17]	D_{ost} = 100 – 300 [11, 61]
Interstitial matrix	14610[1]	55 [62]	238 [17]	-
Cement line	88 [18]	6 [21]	163 [21]	E_{cem} = 5 [11]
Haversian canal	-	-	-	D_{hav} = 20 – 90 [63]

1-Interstitial matrix is considered a more mineralised tissue than osteons [16,17]. Its Young's modulus is often estimated as 10-15% higher than for osteons: 13290MPa·1.1 = 14610 MPa.

In what follows, several numerical models (simplified and realistic) are solved. Fracture is modelled by means of the PNM and using the crack propagation criterion

proposed above, which enables the estimation of the orientation angle of each crack path in a heterogeneous material.

3.2.1. Fracture in simplified geometries (*one-osteon* model) of cortical bone

In this work, we have carried out simulations of simplified osteon morphologies in order to check the numerical prediction of crack paths. Here, crack paths obtained with the PNM and the proposed crack orientation criterion are compared with the ones predicted by XFEM provided by Abaqus and the results obtained by other authors in literature. Solving simplified numerical problems is useful to show the PNM capabilities to predict the crack path in fracture problems within heterogeneous materials, such as cortical bone. In this case, several models with different osteon distributions were developed. These models reproduce a three-point bending test with specimen fracture, since this kind of experiment is usually applied to cortical bone testing in order to measure its stiffness [11]. As presented in Section 1, the crack path is expected to grow mainly through the interstitial matrix and along cement lines, but rarely crossing osteons.

The two different simplified cortical bone models are three-point bending test specimens considering one circular osteon in the mid-plane and two circular osteons off-centred.

The specimen dimensions of the *one-osteon* model are 640 μm × 240 μm. A sketch of the model is shown in Fig. 9a. The osteon is located in the mid-section of the specimen and its morphology is defined by D_{ost}=200 μm and D_{hav}=50 μm surrounded by a cement line of thickness e_{cem}=5 μm. The specimen is supported at two points, separated by a distance of 560 μm. A centred load is applied at the top side with a magnitude of F=20 N. This load is similar to the loads reported in this kind of tests [27]. Plane strain

conditions have been assumed, using quadrilateral elements with full integration (CPE4 in Abaqus). The element size is about 5 μm in order to match the cement line dimensions. The number of elements is approximately 7000. The mechanical properties of the different components are defined in accordance to the literature values summarized in Table 1.

Several authors have developed this kind of simplified models using the XFEM implementation available in Abaqus in combination with the MTS criterion, which was initially conceived for homogeneous materials [27,29-31]. Here, we present a comparison between this procedure and the one proposed in this work. The simulations using the XFEM provided by Abaqus are applied with the Virtual Crack Closure Technique (VCCT) [64] available in Abaqus/Standard with critical energies for each component summarized in Table 1. The angle prediction is based on the MTS criterion.

In this example, an initial crack is located at the lower side of the specimen (marked in red colour in Fig. 9a). The crack growth increment has been set equal to one element size. This small crack increment enables an accurate prediction of the crack path.

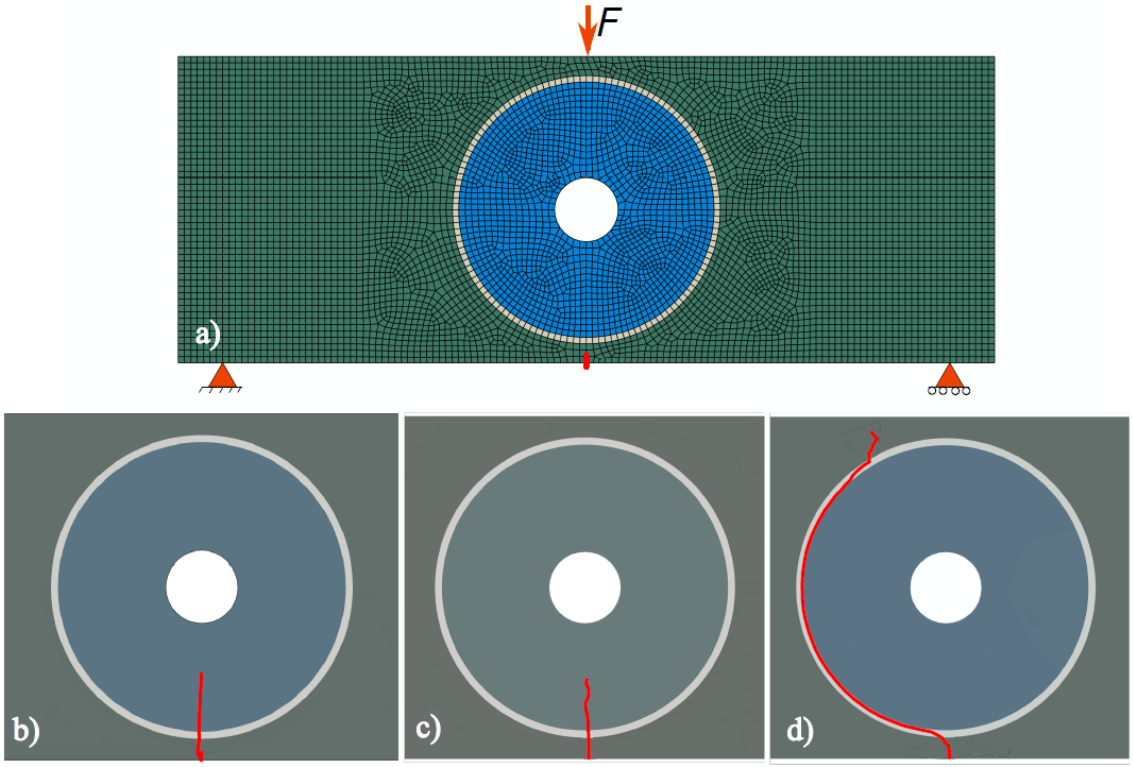

Figure 9. *One-osteon* model in a three-point bending test. a) Geometry and mesh of the test with one centred osteon. b) Crack path obtained through XFEM and MTS criterion available in Abaqus. c) Crack path obtained through PNM and MTS criterion. d) Crack path obtained through PNM and the criterion for heterogeneous materials proposed in this work.

Figs. 9b, 9c and 9d show the different results for the crack path depending on the procedure and criteria used. Note that the fracture paths obtained when the MTS criterion is used (Figs. 9b and 9c) are approximately straight, crossing the cement line and the inner part of osteon, regardless the different mechanical properties of the constituents, which do not seem to affect the crack path computation. This does not match the experimental results shown by other authors, in which cracks mainly grow through the interstitial matrix and along the cement line. We observe that the simple implementation of the MTS criterion cannot discriminate the low ultimate stress of the cement line. On the contrary, the use of the proposed implementation of the PNM and the crack orientation criterion for heterogeneous materials, leads to a more realistic fracture path that takes into account

the heterogeneities within the microstructure (see Fig. 9d). In this case, high shear stresses and a low ultimate stress in the cement line entail crack propagation along it. At the end of the crack propagation, stresses in the interstitial matrix become high enough to divert the fracture from the cement line. Note that in our simulations the crack growth is quasistatic because we assume that the critical load has been reached, as in e.g. [50]. The objective of the numerical examples is to ascertain the proper orientation path considering the heterogeneity of the media.

3.2.2. Fracture in simplified geometries with several osteons

In this subsection, results for some simplified models with several osteons are presented. In the first one, the microstructural morphology of the cortical bone specimen is composed of two osteons and the specimen is subjected to three-point bending test conditions (a sketch of the problem is shown in Fig. 10a). The specimen dimensions are 1000 μm × 400 μm. Close to the mid-section of the specimen two circular osteons are located, with the following dimensions: D_{ost1}=200 μm, D_{hav1}=50 μm, D_{ost2}=120 μm, D_{hav2}=60 μm. Both osteons are surrounded by the cement line of thickness e_{cem}=5 μm. The distance between supports is 870 μm. As in the previous example, a centred load of F=20 N [27] is applied at the top side. Plane strain is assumed, using element type CPE4 in Abaqus. The element size is about 5 μm and the mesh consists of approximately 9900 elements.

The same model is analysed using the XFEM implementation and the MTS criterion available in Abaqus/Standard, and compared with our implementation of the PNM with the heterogeneous material criterion proposed in this work. In this case, the initial crack is located off-centred with respect to the mid-section, as shown in Fig. 10a in red colour.

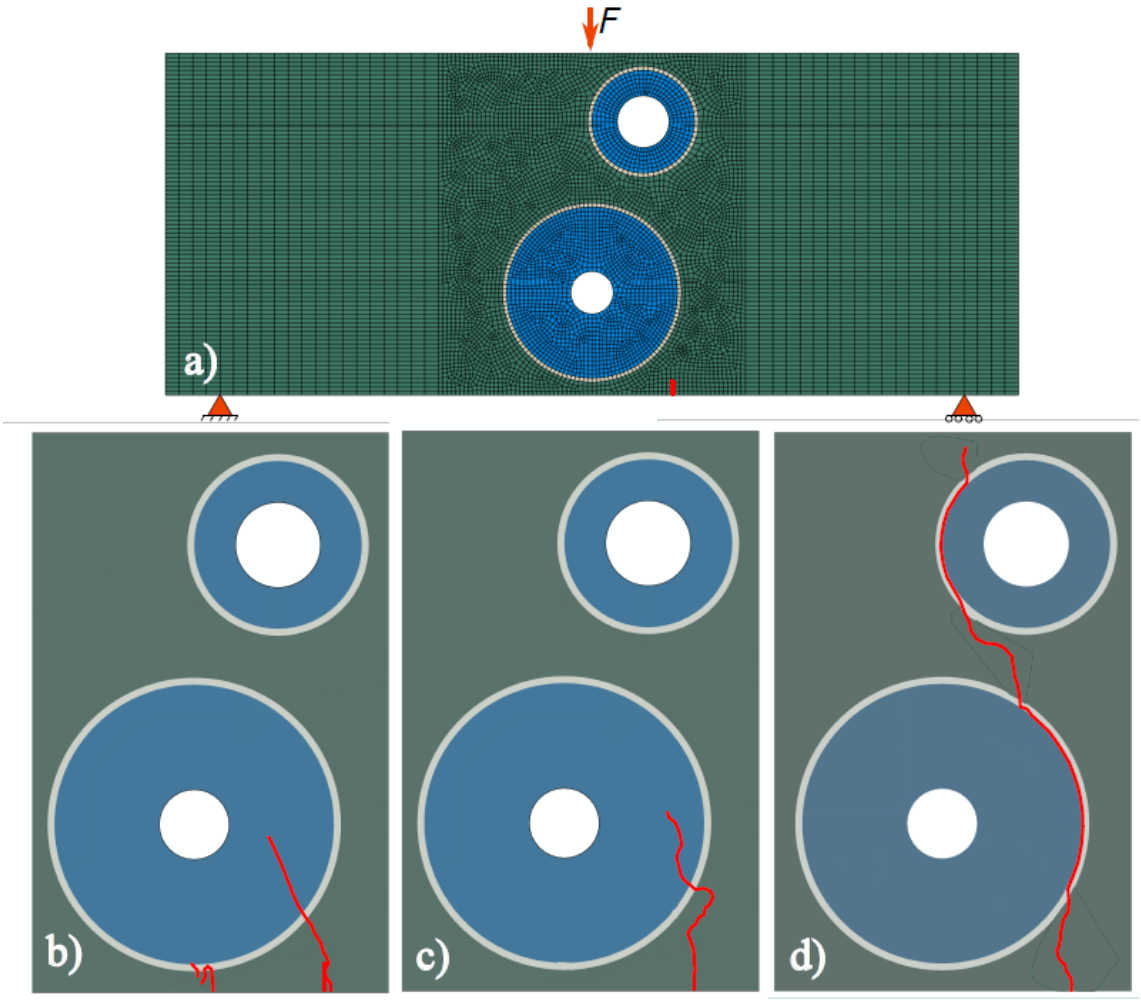

Figure 10. Two osteon model in a three-point bending test. a) Scheme and mesh of the test with two osteons. b) Crack path obtained through XFEM and MTS criterion available in Abaqus. c) Crack path obtained through PNM and MTS criterion. d) Crack path obtained through PNM and the criterion for heterogeneous materials proposed in this work.

Fig. 10d shows that realistic fracture paths can be obtained through PNM and the crack orientation criterion proposed for heterogeneous materials. By using our proposal, the crack path follows the cement line, until stresses in the interstitial matrix are high enough to make it leave the cement line. In the same fashion, the fracture path reaches the second osteon and grows through its cement line. On the contrary, the XFEM method and the PNM combined with the MTS criterion lead to unrealistic fracture paths, Fig. 10b

and 10c, as the crack paths cross cement lines reaching the osteon, regardless the different material properties of each region.

The next step in our analyses is to perform simulations carried out by other authors in simplified geometries. As explained in Section 1, several authors have simulated crack propagation in cortical bone with results which do not agree well with experimental evidence. In the work by Abdel *et al.* [31], authors simulate the fracture of a small cortical bone specimen, simplifying the geometry of osteons to cylinders. In their model, several osteons are positioned in a random distribution, with different diameter sizes. The numerical model has dimensions of 700 μm × 525 μm. Fig. 11b shows the osteon distribution and the boundary conditions that correspond to a tensile traction of the specimen. A plane strain condition is assumed. The element size is approximately 5 μm and the mesh consists of 18600 elements. The tensile traction applied to the right side is equivalent to a 2 N force, as in the original work [31]. An initial crack is located at the bottom of the sample and is marked in yellow colour in Fig. 11b. Abdel *et al.* simulated the problem using XFEM and the MTS criterion as available in Abaqus, obtaining a fracture path that crosses osteons, see Fig. 11a. The path growth does not seem to be affected by the cement line presence and its low stiffness and resistance. By using the XFEM implementation and MTS criterion available in Abaqus, the crack path is mainly determined by the position and size of the Havers canal, which act as stress raisers, despite the material heterogeneities.

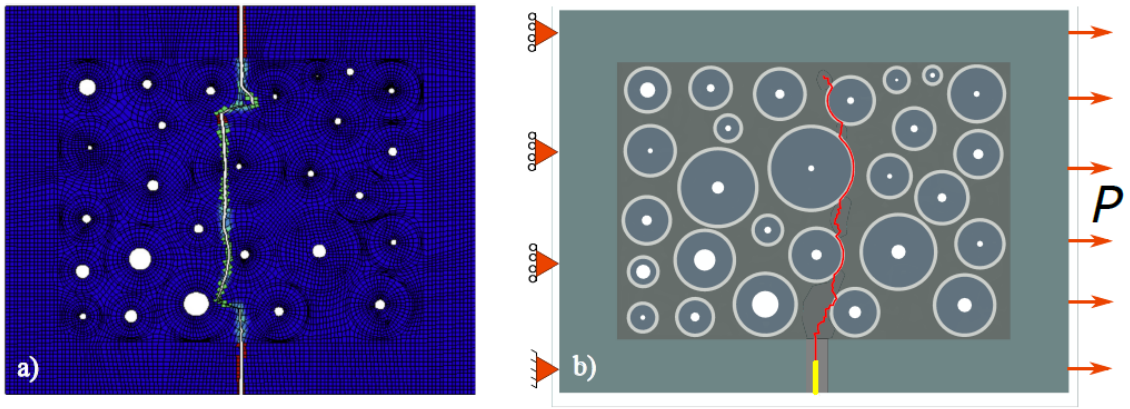

Figure 11. Several osteon model presented by Abdel *et al.* [31]. a) Results obtained by Abdel *et al.* with XFEM and MTS criterion available in Abaqus. Reprinted from [31] with permission of Elsevier. b) Boundary conditions of the problem and results obtained with our implementation of the PNM and the criterion for heterogeneous materials proposed in this work. The initial crack segment is marked in yellow colour.

Fig. 11b shows the crack path prediction when simulated with our PNM implementation and the crack orientation criterion for heterogeneous materials proposed in this work. Initially, the crack growth is ortogonal to the traction direction. After a few steps, the crack is affected by the presence of the first osteon to the rigth and reaches its cement line. The crack path continues along the cement line until stresses become higher in the interstitial matrix. This sequence of events is repeated during the simulation, leading to a more realistic crack path than the one predicted by the XFEM and MTS criterion as available in Abaqus.

3.2.3. Realistic microstructural modelling of crack propagation in cortical bone compared to experimental results obtained by other authors

Once the crack orientation criterion proposed in this work has been tested in different analysis with simplified geometries, a real cortical bone problem is modelled in this section. Several authors have developed experimental tests in cortical bone, observing a crack path mainly growing along cement lines. We aim to reproduce numerically the

experimental work carried out by [27], where authors calculated the local stress intensity factor in cortical bone of a human femur. In this work, Budyn *et al.* obtained experimental fractures in microsamples of bone and modelled them as numerical paths through XFEM, calculating the stress intensity factors at the crack tip.

Here, we model the specimen coded *w06003* by Budyn *et al.* and shown in Fig. 12a, reproducing its real geometry at the microscale. Fig. 12b shows the boundary conditions of the experimental test, and a detail of the crack path obtained by Budyn *et al*. [27]. The specimen dimensions are 6 mm × 2 mm, with an area of interest of 380 μm × 1100 μm, detailed in Fig. 12b. A small notch was generated in the bottom side of the specimen, in order to induce crack initiation. The applied load was set to F=26N, i.e. the same fracture load obtained experimentally for this specimen [27]. In this model, plane strain is assumed, the element size in the area of interest is approximately 5 μm and the mesh consists of approximately 27400 elements.

The specimen geometry and the osteon distribution has been defined through points and splines by means of a Python script. Although the whole specimen was modelled, we only consider the osteon distribution in the zone of interest. Out of the red rectangle marked in Fig. 12b we consider a homogenized material. An initial crack was located at the notch tip.

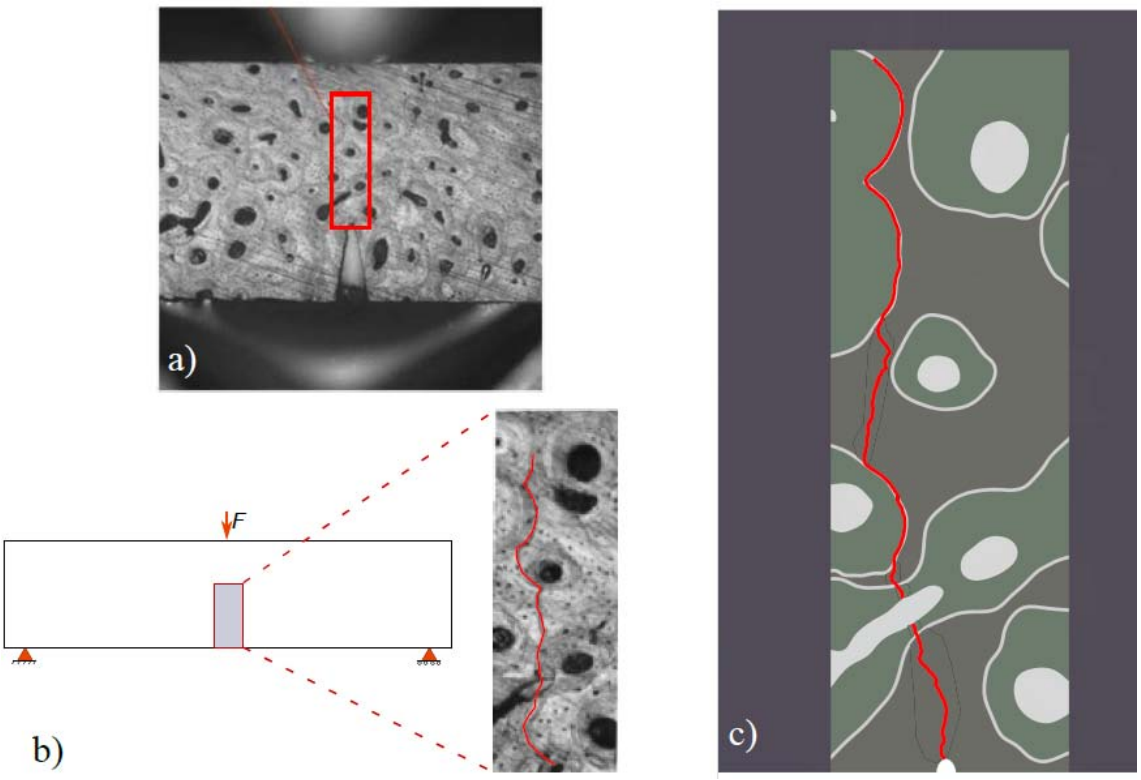

Figure 12. Problem analysed by Budyn *et al.* [27]. a) Notched specimen showing the area of interest Reprinted from [27] with permission of John Wiley and Sons. b) Boundary conditions of the problem, detailed view of the fractured area and experimental crack path marked in red as obtained by [27]. Reprinted from [27] with permission of John Wiley and Sons. c) Crack path prediction obtained through the PNM and orientation criterion for heterogeneous materials proposed in this work.

The implementation of the PNM together with the proposed crack orientation criterion was used to carry out the simulation. In the experimental test performed by Budyn *et al.* [27], the crack path mainly surrounded osteons along their cement lines (Fig. 12b).

The numerical results show an acceptable prediction of the experimental fracture path (Fig. 12c) with slight differences from the observed results. These differences are mainly due to the difficulty when modelling the complex microstructure of a real cortical bone sample at the microscale. Besides the difficulties of defining the borders of some of the osteons, other microdetails, such as microporosity, lacunae (see Fig. 12b) are not

accounted for in the numerical model. Nevertheless, the predicted crack path can be considered realistic and it is in good agreement with experimental evidence. This shows that a numerical model consisting of osteons, interstitial matrix, Havers canals and cement lines may be sufficient to simulate crack propagation in cortical bone at the microscale. Thus, the application of the implemented PNM and the proposed crack orientation criterion has proved to capture adequately the interaction between the constituents of cortical bone. This shows the importance of considering cortical bone as a heterogeneous material at the microscale.

4. Conclusions

The numerical modelling of crack growth in cortical bone at the microstructural level has been successfully accomplished through a user implementation of the PNM in the commercial code Abaqus combined with a dedicated orientation criterion for heterogeneous materials. The PNM allows representing the displacement discontinuity across crack faces avoiding the need of element sides to conform to the crack faces and the need of remeshing to simulate crack propagation. The proposed crack orientation criterion has proven to be essential, as it takes into account the heterogeneity of the constituents to determine the direction of crack propagation when a crack encounters a material interface. This aspect is not currently considered by commercial implementations of the XFEM in Abaqus and has led to unrealistic crack growth predictions in the literature.

Previously, the method has been validated through LEFM problems with known solutions of reference, both in mode I and mixed mode. The implementation has proven to be sufficiently accurate when an appropriate mesh is used, with errors in SIFs estimation of about 1%.

After its validation, the PNM has been applied to model bone fracture at the micro scale. At this scale, the need of a crack propagation criterion that takes into account the heterogeneity of the microstructure is evidenced. The criterion is based on the prediction of interface damage considering the stress distribution ahead the crack tip in combination with the MTS criterion. This leads to crack growth predictions that are in good agreement with experimental observations, in contrast to other results found in the literature.

Several examples with idealized osteons have been modeled using the PNM and the proposed crack orientation criterion and also a cortical bone microsample reported by other authors in the literature. As expected, crack paths mainly grow and propagate through the weakest interface (cement line) and do not tend to cross osteons. Thus, the crack growth predictions agree with the observed experimental crack paths. The presented results show the importance of considering the heterogeneity, in contrast to other current commercial implementations. Furthermore, the procedure can be applied to model crack growth in other heterogeneous structures.

5. Acknowledgements

The authors gratefully acknowledge the funding support received from the Spanish Ministry of Economy and Competitiveness and the FEDER operation program in the framework of the projects DPI2013-46641-R, DPI2017-89197-C2 and RTC-2015-3887-8 and also from the Generalitat Valenciana through the Programme PROMETEO 2016/007.

6. References

1. F. Libonati, L. Vergani, Understanding the structure–property relationship in cortical bone to design a biomimetic composite, Comp. Struct. 139 (2016) 188-198.
2. D.T. Gold. The nonskeletal consequences of osteoporotic fractures: Psychologic and social outcomes, Rheum. Dis. Clin. N. Am. 27(1) (2001) 255-262.
3. J. Kanis, O. Johnell, Requirements for DXA for the management of osteoporosis in Europe, Osteoporosis Int. 16 (2005) 229-238.
4. W. Li, D. Lin, C. Rungsiyakull, S. Zhou, M. Swain, Q. Li, Finite element based bone remodeling and resonance frequency analysis for osseointegration assessment of dental implants, Finite Elem. Anal. Des. 47 (2011) 898-905.
5. W. Yi, C. Wang, X. Liu, A microscale bone remodeling simulation method considering the influence of medicine and the impact of strain on osteoblast cells, Finite Elem. Anal. Des. 104 (2015) 16-25.
6. J.Y. Rho, L. Kuhn-Spearing, P. Zioupos, Mechanical properties and the hierarchical structure of bone, Med. Eng. and Phys. 20 (1998) 92-102.
7. J.D. Currey, The structure and mechanics of bone, J. Mater. Sci. 47 (2012) 41-54.
8. T. Burczynski, W. Kus, A. Brodacka, Multiscale modeling of osseous tissues, J. Theor. App. Mech. 48(4) (2010) 855-870.
9. A. Ural, S. Mischinski, Multiscale modeling of bone fracture using cohesive finite elements, Eng. Fract. Mech. 103 (2013) 141-152.
10. S.H. Kim, S.H. Chang, H.J. Jung, The finite element analysis of a fractured tibia applied by composite bone plates considering contact conditions and time varying properties of curing tissues, Compos. Struct. 92 (2010) 2109–18.
11. S.C. Cowin, Bone mechanics handbook, CRC Press, Boca Raton, Florida, 2001.

12. T.M. Keaveny, W.C. Hayes, A 20-year perspective on the mechanical properties of trabecular bone, Transactions of the ASME 115 (1993) 534-542.
13. T.M. Keaveny, E.F. Morgan, G.L. Niebur, O.C. Yeh. Biomechanics of trabecular bone, Annu. Rev. Biomed. Eng. 3 (2001) 307-333.
14. K. Piekarski, Analysis of bone as a composite material, Int. J. Eng. Sci. 11(6) (1973) 557-558.
15. D. Taylor, J.G. Hazenberg, T.C. Lee, Living with cracks: damage and repair in human bone, Nat. Mater. 6 (2007) 263–268.
16. J.Y. Rho, J.D. Currey, P. Zioupos, G.M. Pharr, The anisotropic Young's modulus of equine secondary osteones and interstitial bone determined by nanoindentation, J. Exp. Biol. 204(10) (2001) 1775-1781.
17. S. Li, A. Abdel-Wahab, D. Emrah, V.V. Silberschmidt, Fracture process in cortical bone: X-FEM analysis of microstructured models, Int. J. Fract. 184 (2013a) 43-55.
18. S. Nobakhti, G. Limbert, P.J. Thurner, Cement lines and interlamellar areas in compact bone as strain amplifiers contributors to elasticity, fracture toughness and mechanotransduction, J. Mech. Behav. Biomed. Mater. 29 (2014) 235-251.
19. A. Vercher, E. Giner, C. Arango, J.E. Tarancón, F.J. Fuenmayor, Homogenized stiffness matrices for mineralized collagen fibrils and lamellar bone using unit cell finite element models, Biomech. Model Mechanobiol. 13(2) (2014) 437–449.
20. D.B. Burr, M.B. Schaffler, R.G. Frederickson, Composition of the cement line and its possible mechanical role as a local interface in human compact bone, J. Biomech. 21 (1988) 939-945.
21. E. Giner, R. Belda, C. Arango, A. Vercher-Martínez, J.E., Tarancón, F.J. Fuenmayor. Calculation of the critical energy release rate G_c of the cement line in

cortical bone combining experimental tests and finite element models, Eng. Fract. Mech. 184 (2017) 168-182.

22. G. Maj, E. Toajari, Osservazioni sperimentali sul meccanismo di resistenza del tessuto osseo lamellare compatto alle azioni meccaniche, Chir. Org. Mov. 22 (1937) 541-557.
23. F.G. Evans, S. Bang, Physical and histological differences between human fibular and femoral compact bone, Studies on the Anatomy and Function of Bone and Joints, Springer, (1966) 142-155.
24. F.G. Evans, Mechanical properties and histology of cortical bone from younger and older men, The Anat. Rec. 185(1) (1976) 1-11.
25. M. Doblaré, J.M. García, M.J. Gómez, Modelling bone tissue fracture and healing: a review, Eng. Fract. Mech. 71(13) (2004) 1809-1840.
26. R.O. Ritchie, J.H. Kinney, J.J. Kruzic, R.K. Nalla, A fracture mechanics and mechanistic approach to the failure of cortical bone, Fatigue Fract. Eng. Mater. Struct. 28(4) (2005) 345-371.
27. E. Budyn, T. Hoc, Analysis of micro fracture in human haversian cortical bone under transverse tension using extended physical imaging, Int. J. Numer. Meth. Eng. 82(8) (2010) 940-965.
28. J.G. Skedros, J.L.Holme, E.G. Vajda, R.D. Bloebaum, Cement lines of secondary osteons in human bone are not minetal-deficient: new data in a historical perspective, Anat. Rec. A. Discov. Mol. Cell. Evol. Biol. 286 (2005) 781-803.
29. E. Budyn, T. Hoc, Multiple scale modeling for cortical bone fracture in tension using X-FEM, Europ. J. Comp. Mech. 16(2) (2007) 213-236.

30. E. Budyn, T. Hoc, J. Jonvaux, Fracture strength assessment and aging signs detection in human cortical bone using an X-FEM multiple scale approach, Comp. Mech. 42(4) (2008) 579-591.
31. A. Abdel-Wahab, A.R. Maligno, V.V. Silberschmidt, Micro-scale modelling of bovine cortical bone fracture: Analysis of crack propagation and microstructure using X-FEM, Comp. Mat. Sci. 52(1) (2012) 128-135.
32. M. Wang, X. Gao, A. Abdel-Wahab, S. Li, E.A. Zimmermann, C. Riedel, B. Busse, V.V. Silberschmidt, Effect of micromorphology of cortical bone tissue on crack propagation under dynamic loading, EPJ Web of Conferences 94 (2015).
33. L. Vergani, C. Colombo, F. Libonati, Crack propagation in cortical bone: a numerical study, Proc. Mat. Science 3 (2014) 1524-1529.
34. A. Idkaidek, S. Koric, I. Jasiuk, Fracture analysis of multi-osteon cortical bone using XFEM, Comput. Mech. (2017), *in press*
35. X.E. Guo, L.C. Li, S.A. Goldstein, Micromechanics of osteonal cortical bone fracture, Transactions of the ASME 120 (1998) 112-117.
36. L. Lin, X. Wang, X. Zeng, An improved interfacial bonding model for material interface modelling, Eng. Fract. Mech. 169 (2017) 276-291.
37. F.A.M. Pereira, M.F.S.F de Moura, N. Dourado, J.J.L. Morais, F.G.A. Silva, M.I.R. Dias, Bone fracture characterization under mixed-mode I+II loading using the MMB test, Eng. Fract. Mech. 166 (2016) 151-163.
38. F.A.M. Pereira, J.J.L. Morais, M.F.S.F de Moura, N. Dourado, M.I.R. Dias, Evaluation of bone cohesive laws using an inverse method applied to the DCB test, Eng. Fract. Mech. 96 (2012) 724-736.
39. B.N. Cox, Q. Yang, Cohesive zone models of localization and fracture in bone, Eng. Fract. Mech. 74 (2007) 1079-1092.

40. F.J. Vernerey and M. Kabiri, An adaptive concurrent multiscale method for microstructured elastic solids. Comput. Methods in Appl. Mech. Eng., 241–244 (2012) 52-64.
41. F.J. Vernerey and M. Kabiri, Adaptive concurrent multiscale model for fracture and crack propagation in heterogeneous media. Comput. Methods in Appl. Mech. Eng., 276 (2014) 566-88.
42. F.V. Souza and D.H. Allen, Modeling the transition of microcracks into macrocracks in heterogeneous viscoelastic media using a two-way coupled multiscale model, Int. J. Solids. Struct., 48 (2011) 3160-75.
43. S. Li, A.A. Abdel, V.V. Silverschmidt, Analysis of fracture processes in cortical bone tissue, Eng. Fract. Mech. 110 (2013b) 448-458.
44. A. Hansbo, P. Hansbo, A finite element method for the simulation of strong and weak discontinuities in solid mechanics, Comput. Methods Appl. Mech. Eng. 19(33) (2004) 3523-3540.
45. C. Wang, X. Xu, An extended phantom node method study of crack propagation of composites under fatigue loading, Comp. Struct. 154 (2016) 410-418.
46. J.H. Song, P Areias, T. Belytschko, A method for dynamic crack and shear band propagation with phantom nodes, Int. J. Numer. Meth. Eng. 67 (2006) 868-893.
47. A. Ahmed, L.J. Sluys, A phantom node formulation for modeling coupled adiabatic–isothermal cracking in FRP composites, Comput. Methods Appl. Mech. Eng. 278 (2014) 291-313.
48. N. Moës, J. Dolbow, T. Belytschko, A finite element method for crack growth without remeshing, Int. J. Numer. Meth. Engng. 46 (1999) 131-150.
49. M.F. Kanninen, C.L. Popelar, Advanced Fracture Mechanics, Oxford University Press, Oxford, 1985.

50. E. Giner, N. Sukumar, J.E. Tarancón, F.J. Fuenmayor, An Abaqus implementation of the extended finite element method, Eng. Fract. Mech. 76(3) (2009) 347-368.
51. E. Giner, F.J. Fuenmayor, L. Baeza, J.E. Tarancón, Error estimation for the finite element evaluation of G_I and G_{II} in mixed-mode linear elastic fracture mechanics. Finite Elem. Anal. Des. 41 (2005) 1079-1104.
52. D. Hull, T.W. Clyne, An introduction to composite materials, Cambridge University Press, 1996.
53. E. Giner, C. Arango, A. Vercher, F.J. Fuenmayor, Numerical modelling of the mechanical behaviour of an osteon with microcracks, J. Mech. Behav. Biomed. Mater. 37 (2014) 109-124.
54. M. Marco, M. Rodríguez-Millán, C. Santiuste, E. Giner, M.H. Miguélez, A review on recent advances in numerical modelling of bone cutting, J. Mech. Behav. Biomed. Mater. 44 (2015) 179-201.
55. M. Marco, E. Giner, R. Larraínzar, J.R. Caeiro, M.H. Miguélez, Numerical modelling of femur fracture and experimental validation using bone simulant, Ann. Biomed. Eng. 45(10) (2017) 2395-2408.
56. D.T. Reilly and A.H. Burstein, The elastic and ultimate properties of compact bone tissue, J. Biomech. 8(6) (1975) 393-405.
57. P.K. Zysset, X.E. Guo, C.E. Hoffler, K.E. Moore, S.A. Goldstein, Elastic modulus and hardness of cortical and trabecular bone lamellae measured by nanoindentation in the human femur, J. Biomech., 32(10) (1999) 1005–1012.
58. J.Y. Rho, T.Y. Tsui, G.M. Pharr, Elastic properties of human cortical and trabecular lamellar bone measured by nanoindentation. Biomaterials, 18(20) (1997) 1325–30.

59. M.G. Ascenzi, N.P. Kawas, A. Lutz, D. Kardas, U. Nackenhorst, J.H. Keyak, Individual-specific multi-scale finite element simulation of cortical bone of human proximal femur, J. Comput. Phys. 244 (2013) 298–311.
60. X.N. Dong and X.E. Guo, Prediction of cortical bone elastic constants by a two-level micromechanical model using a generalized self-consistent method, J. Biomech. Eng. 128(3) (2006) 309-316.
61. A. Ascenzi, E. Bonucci, The shearing properties of single osteons, The Anat. Rec., 172(3) (1973) 499-510.
62. C. Arango, Ph.D. thesis: Study of the mechanical behavior of cortical bone microstructure by the finite element method, Universitat Politècnica de València, Valencia, Spain, (2016).
63. M. Ascenzi, J.M. Kabo, M. Andreuzzi, Mathematical modeling of human secondary osteons, Scanning 26(1) (2004) 25-35.
64. E.E. Gdoutos, Fracture Mechanics: An Introduction. Solid Mechanics and its Applications, Kluwer Academic Publishers, Dordrecht, The Netherlands, 1993.